Materials Research Express

PAPER

Optical and electrical properties of thermally co-evaporated $SnS_{1-x}Se_x$ alloy films

RECEIVED
9 July 2019

REVISED
24 August 2019

ACCEPTED FOR PUBLICATION
2 September 2019

PUBLISHED
11 September 2019

K Saritha[1], **S Rasool**[1], **K T Ramakrishna Reddy**[1], **M S Tivanov**[2], **A M Saad**[3], **A V Trofimova**[2] and **V F Gremenok**[4]

[1] Department of Physics, Sri Venkateswara University, Tirupati-517 502, India
[2] Faculty of Physics, Belarusian State University, 220030 Minsk, Belarus
[3] Al-Balqa Applied University, Salt 19117, Jordan
[4] Scientific and Practical Materials Research Centre, National Academy of Sciences, 220072 Minsk, Belarus

E-mail: ktrkreddy@gmail.com

Keywords: $SnS_{1-x}Se_x$ thin films, thermal co-evaporation, band gap energy, Urbach energy, resistivity, photosensitivity

Abstract

The paper presents studies of optical and electrical properties of $SnS_{1-x}Se_x$ (x = 0.26–0.31) thin films deposited on glass substrates using thermal co-evaporation technique at different substrate temperatures, 200 °C–350 °C. The as-deposited films were characterized by the energy dispersive spectroscopy, X-ray diffractometry, scanning electron microscopy, optical transmission and reflection spectroscopy, four-probe resistivity and photoconductance measurements. The results have shown that deposited films can be used as absorber layers in thin film solar cell applications, and the optimal substrate temperature for the deposition is 300 °C.

1. Introduction

For several decades, a variety of metal chalcogenide semiconductors were studied and investigated for solar cell applications, but only few are identified as better materials for photo conversion process. Among them, only few semiconductors such as CdTe and $Cu(InGa)Se_2$ (CIGSe) were extensively investigated and proved as better materials for solar energy conversion with reported efficiencies over 20% [1, 2]. Also, these materials are currently well-established with commercialized technologies in the solar industry. However, the disadvantages in these technologies are toxicity of Cd and scarcity of Te in CdTe and less availability of In and Ga in CIGS. This causes health issues in case of CdTe-based solar cells and conflict between supply and demand of materials for large scale power generation that restrict the mass production of CIGS-based solar cells in near future. Hence, alternative earth-abundant and non-toxic materials with an easy controllability of stoichiometry are of interest for future photovoltaics. In this context, Cu_2ZnSnS_4 (CZTS) and $Cu_2ZnSnSe_4$ (CZTSe) have been considered as an alternative to CIGS and CdTe, since these materials possess earth abundant and less toxic constituent elements. However, the conversion efficiencies achieved using these two materials were lower than CdTe and CIGS technologies [3–6]. The highest power conversion efficiency recorded so far in case of CZTS and CZTSe-based solar cells were 9.2% [7] and 11.6% [8] respectively, which were less, compared to 12.6% efficiency achieved on mixed sulfo-selenide CZTSSe-based solar cells [9]. Though it is a potential solar absorber material, the precise control of composition and structural transitions are difficult due to the presence of more number of elements. Therefore, simple ternary / binary sulfo-selenide compounds are of great interest for solar cell application. In this context, tin sulfoselenide ($SnS_{1-x}Se_x$) has attracted the researcher's interest because of its suitable and tunable physical properties.

Tin sulfoselenide is a p-type semiconductor capable of absorbing major portion of solar energy with high optical absorption coefficient ($\sim 10^5$ cm^{-1}) and tunable band gap energy [10]. Moreover, its constituent elements are earth abundant and low toxic. Hence, SnSSe is a promising material for low cost thin film solar cell development. It mostly crystallizes in orthorhombic crystal structure and exhibits the properties of both SnS and SnSe [11]. Upto now, very limited work has been carried out on the synthesis and characterization of SnSSe in

different forms such as single crystals [12], nanocrystals [13], nanosheets [14] and thin films [15]. SnSSe thin films have been deposited by chemical and physical techniques mainly using electrodeposition [16], screen printing [17], thermal evaporation [18] and chemical bath deposition [19]. Although, few groups have investigated on SnSSe thin films followed by characterization, however, the reported data is very meagre and needs thorough and detailed investigation of different physical properties in relation to growth conditions. Recently, Barrios-Salgado *et al* prepared cubic SnS_xSe_{1-x} ($x = 0.65$) layers by chemical bath deposition and also developed a solar cell in the configuration of FTO/CdS/Sb_2S_3/SnS_xSe_{1-x}/C-Ag that showed a photo conversion efficiency of 1.15% [20].

In the present work, $SnS_{1-x}Se_x$ thin films were deposited using thermal co-evaporation method for the first time, which is a suitable technique to deposit compound or alloy materials with flexibility to control the film composition. In vacuum techniques, substrate temperature is one of the important parameters to be optimized to grow high quality films. Therefore, $SnS_{1-x}Se_x$ films were deposited at different substrate temperatures (T_s), 200 °C–350 °C and its influence on the optical, electrical and photoconductive behaviour of as-deposited films was investigated and reported.

2. Experimental and characterization details

$SnS_{1-x}Se_x$ thin films were deposited on soda lime glass substrates using thermal co-evaporation technique (HHV BC 300 model box coater). For deposition of layers, SnS (Alfa Aesar, 99.7%) and Se (Sigma Aldrich, 99.99%) powders were co-evaporated at a vacuum of 5×10^{-5} mbar. The layers were deposited at different substrate temperatures, $T_s = 200, 250, 300, 350$ °C, while other growth parameters including source to substrate distance (13 cm) and deposition rate (~20 Å s^{-1}) were maintained as constant. The energy dispersive X-ray spectroscopy (EDS) was performed to identify the chemical composition of the films. The structural behaviour of $SnS_{1-x}Se_x$ films was analyzed using Ultima IV X-ray diffractometer in the grazing incidence (1°) diffraction geometry (GIXD) with Cu Kα radiation source ($\lambda = 1.5406$ Å). The surface morphological details of the layers were investigated using scanning electron microscope (SEM) (S-4800, Hitachi). Photon RT spectrophotometer (Essent Optics) was used to analyze the optical properties using unpolarized light at room temperature in the wavelength range, 400–1600 nm. The type of electrical conduction and resistivity of as-deposited $SnS_{1-x}Se_x$ films were investigated using hot probe and four probe techniques respectively. In addition, the photoconductivity of the films was examined at thermostatically controlled constant temperature 307 K under LED illumination with radiation wavelength 465 nm and maximum light intensity 3.5 mW cm^{-2}.

3. Results and discussion

3.1. Structural properties

The EDS analysis of $SnS_{1-x}Se_x$ ($x = 0.26, 0.28, 0.30, 0.31$) films formed at different T_s values indicated the presence of Sn, S and Se as constituent elements. Generally in thermal evaporation, the composition of alloys critically depends on factors such as substrate temperature, deposition rate and vapour pressure of elements. In case of $SnS_{1-x}Se_x$ films grown at higher substrate temperatures, a rapid reaction of Se vapour with SnS led to the formation of $SnS_{1-x}Se_x$ phase by replacing S with Se. In addition, the thermodynamical data shows that the vapour pressure of S (1 kPa at 508 K) is much higher compared to Se (1 Pa at 500 K). Therefore, the S content slightly decreases in the films at higher substrate temperatures and Se content increases due to more Se incorporation.

The GIXD patterns of as-deposited $SnS_{1-x}Se_x$ thin films are shown in figure 1, which indicates the polycrystalline nature of the films with a number of planes that are corresponding to $SnS_{1-x}Se_x$ phase with orthorhombic crystal structure. All the presented planes are closely matched with the planes of $SnS_{0.5}Se_{0.5}$ (JCPDS card no.: 48–1225) with a slight shift in the peak positions due to the change in the composition of the as-deposited $SnS_{1-x}Se_x$ layers with variation of substrate temperature. The films exhibited an intense peak at $2\theta = 31.7°$ related to (111) plane as the preferred crystallographic orientation, whose intensity was increased with increase of substrate temperature. The GIXD studies revealed that the crystallinity of the films was enhanced with the increase of substrate temperature. Further, two small peaks related to SnS phase was observed in the films deposited at 350 °C due to desorption of Se atoms at such higher temperatures.

3.2. Morphological studies

The SEM surface morphology pictures of $SnS_{1-x}Se_x$ layers deposited at different substrate temperatures are shown in figure 2. The pictures clearly indicate the effect of substrate temperature on the growth of grains over the substrate surface. From the images, it was noticed that the films were homogeneous and continuous with the grains grown uniformly over the substrate surface without any cracks. Initially, the grains were appeared as

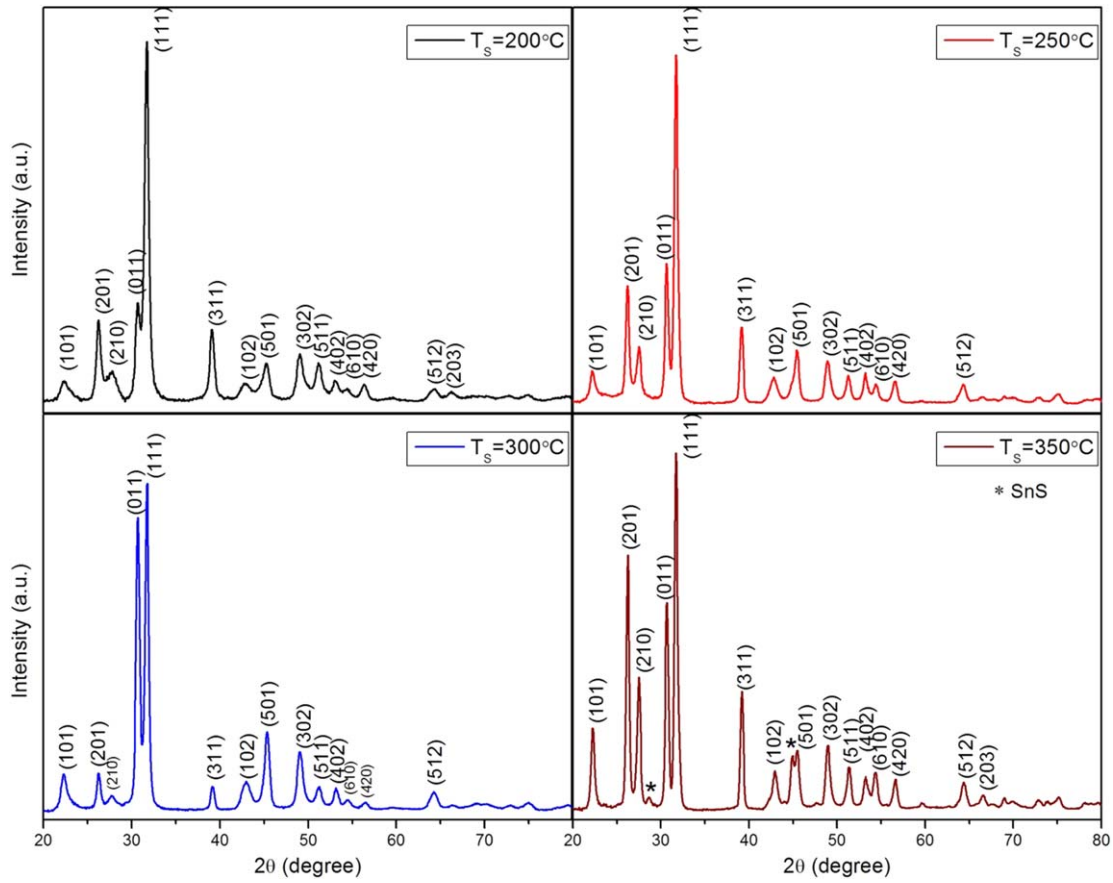

Figure 1. GIXD patterns of $SnS_{1-x}Se_x$ thin films deposited at different T_s.

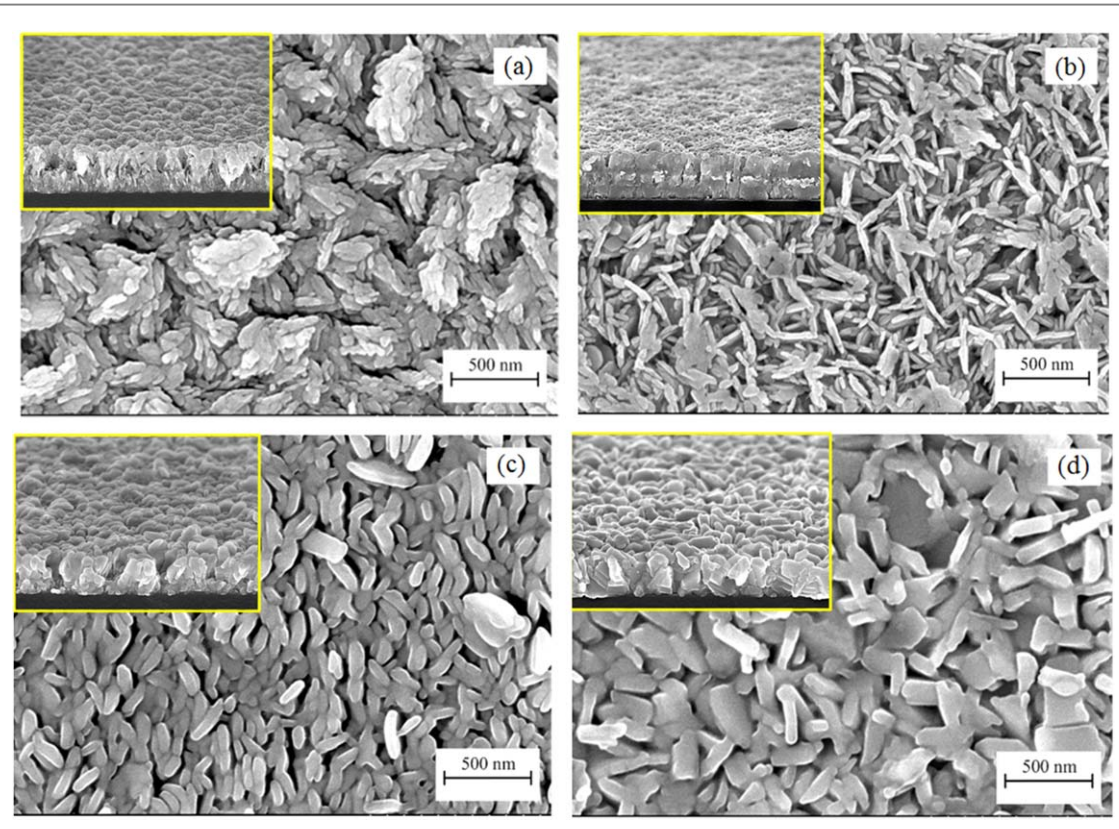

Figure 2. SEM images of $SnS_{1-x}Se_x$ films deposited at: (a) $T_s = 200$ °C, (b) $T_s = 250$ °C, (c) $T_s = 300$ °C and (d) $T_s = 350$ °C.

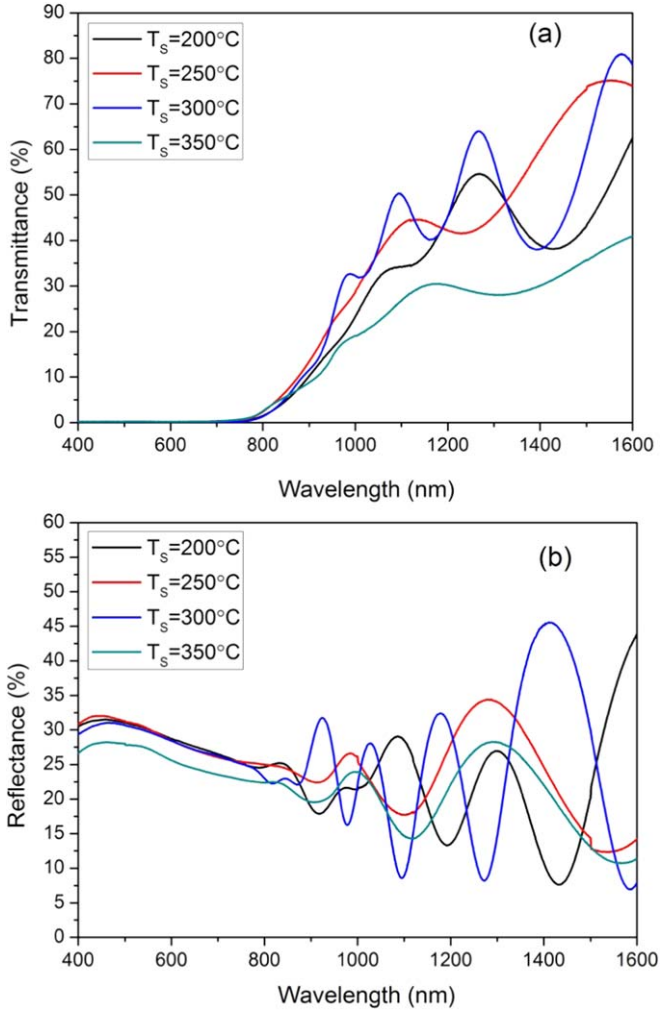

Figure 3. Optical (a) transmittance and (b) reflectance versus wavelength plots of $SnS_{1-x}Se_x$ films.

bunches of cereals for $T_s = 200$ °C. With increase of substrate temperature, the individual cereals were disintegrated into smaller grains that were further grown into larger grains at higher T_s values. From the cross sectional SEM analysis, it was noticed that the grains had columnar growth, where the grains were formed perpendicular to the substrate surface.

3.3. Optical properties

Figure 3 shows the optical transmittance (T) and reflectance (R) spectra of $SnS_{1-x}Se_x$ thin films deposited at different substrate temperatures. The figure depicts that all the films showed very low transmittance and nearly 30% reflectance in the visible region, which indicates that these properties are not significantly influenced by the change in substrate temperature in such wavelength region. The appearance of interference fringes in transmittance spectra indicates that the films had good surface homogeneity and uniformity.

The optical absorption coefficient (α) of the films was calculated using the transmittance (T) and reflectance (R) data by following the relation (1) [21],

$$\alpha = -\frac{1}{t} ln\left(\frac{\sqrt{(1-R)^4 + 4T^2R^2} - (1-R)^2}{2TR^2}\right) \quad (1)$$

where, t is the thickness of the films (~1.0 μm). The dependence of absorption coefficient (α) of as-deposited $SnS_{1-x}Se_x$ films upon the incident wavelength for films formed at different substrate temperatures is shown in figure 4. The analysis revealed that the $SnS_{1-x}Se_x$ films deposited at T_s in the range, 200 °C-300 °C showed high optical absorption coefficient of ~10^5 cm^{-1}, while the films at $T_s = 350$ °C showed ~10^4 cm^{-1} in the visible region and then the absorption decreased gradually with increase of wavelength. The low absorption coefficient observed in the films formed at $T_s = 350$ °C is due to the presence of secondary phase in the layers that led to creation of more localized states in the film [22, 23]. The obtained α value of $SnS_{1-x}Se_x$ films is comparable with the reported values of both SnS and SnSe thin films deposited by thermal evaporation [24, 25].

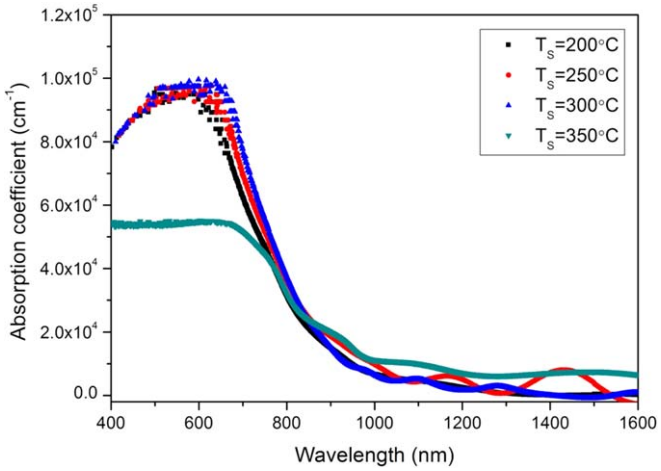

Figure 4. Optical absorption coefficient versus wavelength plots of $SnS_{1-x}Se_x$ layers.

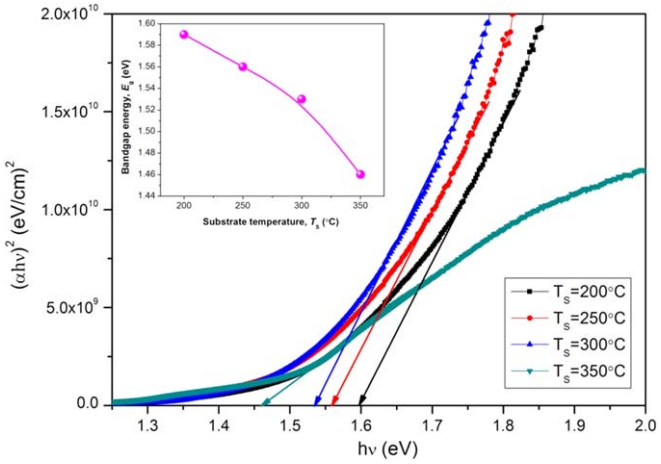

Figure 5. Tauc plots of $SnS_{1-x}Se_x$ films.

Using the values of α and assuming that the band-to-band transition is direct allowed, the optical energy band gap (E_g) of the films can be evaluated from the Tauc relation [26]:

$$(\alpha h\nu)^2 = A(h\nu - E_g), \tag{2}$$

where $h\nu$ is the incident photon energy and A is a constant. The $(\alpha h\nu)^2$ versus $h\nu$ plots for $SnS_{1-x}Se_x$ films deposited at different substrate temperatures are shown in figure 5. The optical band gap energy of the as-deposited films decreased from 1.59 to 1.46 eV with increase of substrate temperature from 200 to 350 °C (see inset figure 5). The decrease in band gap energy with substrate temperature was ascribed to the decreased structural defects, improvement in crystallinity and variation in composition of the films. Similar type of reduction in band gap energy of SnS films with growth temperature was observed and reported by Zhao *et al* [27].

The Urbach energy (E_U) gives the information about the existence of localized states in the band gap region. Their presence is related to the unsaturated bonds or defects in the films. In low photon energy range ($h\nu < E_g$), the absorption coefficient follows the Urbach empirical rule (relation 3).

$$\alpha = \alpha_0 \exp\left[\frac{h\nu}{E_U}\right], \tag{3}$$

where, α_0 is a constant.

The value of E_U can be obtained from the inverse slope of the linear plot of $\ln(\alpha)$ versus $h\nu$ as shown in figure 6 [28]. From the figures, it was observed that the E_U values of $SnS_{1-x}Se_x$ films were decreased with increase of T_s and reached a minimum of $E_U = 178$ meV for $T_s = 300$ °C. This indicates that the substrate temperature plays an important role in reducing the structural defects and localized state density in the band gap region of the

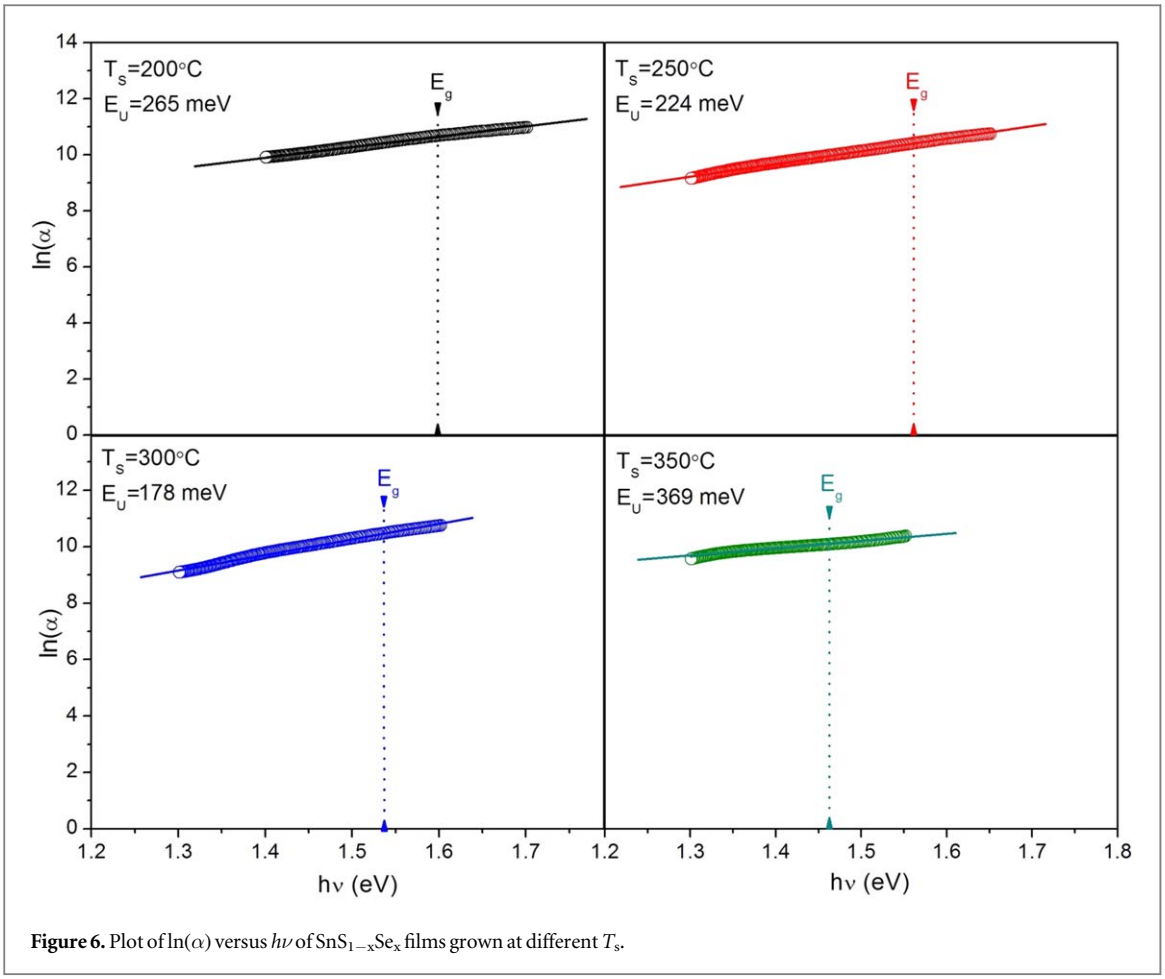

Figure 6. Plot of ln(α) versus $h\nu$ of $SnS_{1-x}Se_x$ films grown at different T_s.

Table 1. Variation in E_U and n values of $SnS_{1-x}Se_x$ films with T_s.

T_s (°C)	200	250	300	350
E_U (meV)	265	224	178	369
n	2.90	2.92	2.93	2.97

films. For further increase of temperature to 350 °C, Urbach energy was increased to 369 meV, indicating the presence of more defect states in the band gap region compared to all other films.

The refractive indices (n) of as-deposited $SnS_{1-x}Se_x$ films were evaluated from optical measurements using the Herve-Vandamme formula (relation 4), in which n is inversely proportional to E_g and A and B are constants equal to 13.6 eV and 3.4 eV respectively [29].

$$n = \left[1 + \left(\frac{A}{E_g + B}\right)^2\right]^{1/2} \tag{4}$$

The obtained refractive index values of $SnS_{1-x}Se_x$ films were slightly increased from 2.90 to 2.97 with increase of T_s. This indicates that the layers became dense with increase in T_s. The variation in n values with respect to substrate temperature is given in table 1. Also, these values are in close agreement with the reported values of Subramanian *et al* [16] for electrodeposited $SnS_{0.5}Se_{0.5}$ films.

The extinction coefficient (k) refers to the loss of incident light inside the material due to scattering and absorption. For the $SnS_{1-x}Se_x$ films, the extinction coefficient was determined using the optical absorption coefficient (α), following the relation (5).

$$k = \frac{\alpha\lambda}{4\pi} \tag{5}$$

Figure 7 shows the variation of extinction coefficient against the wavelength (λ) of incident photon energy for $SnS_{1-x}Se_x$ films. The figure depicts that the extinction coefficient decreases with increase of wavelength.

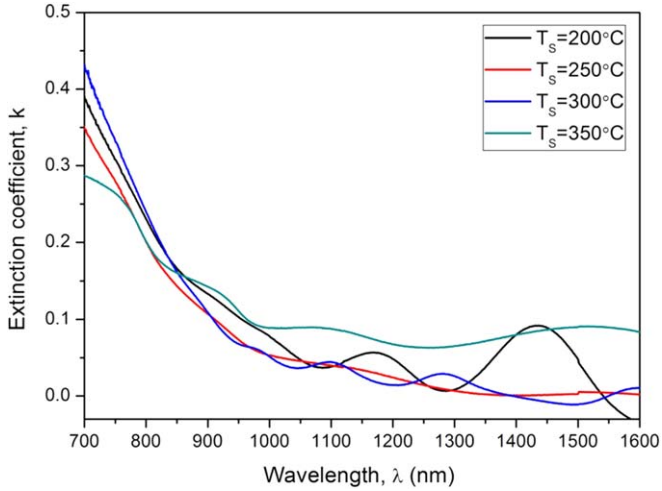

Figure 7. Variation of extinction coefficient, k with wavelength for $SnS_{1-x}Se_x$ films.

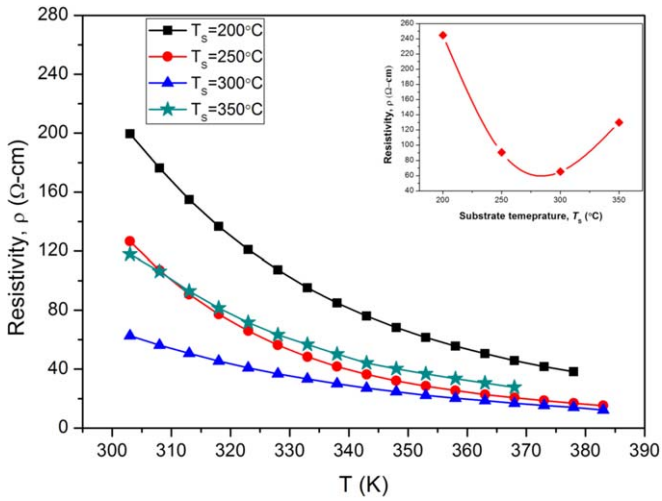

Figure 8. Temperature dependent electrical resistivity of $SnS_{1-x}Se_x$ films deposited at different T_s.

3.4. Electrical properties

The hot probe measurements showed negative voltage values for all the films, indicating p-type electrical conductivity in $SnS_{1-x}Se_x$ films. From the four probe measurements, the resistivity (ρ) of the films was decreased with increase of temperature as shown in figure 8, which confirms the semiconducting nature of the films. Further, this study revealed that there is a considerable effect of substrate temperature on electrical resistivity (ρ) of the films, see inset of figure 8. The resistivity (ρ) of the films was decreased with increase of substrate temperature and reached a minimum of 65.2 Ω-cm at $T_s = 300$ °C and then increased to 130.0 Ω-cm with further rise in T_s. The decrease in resistivity of the films with substrate temperature represents the better crystallinity of the films and the increase in resistivity at higher substrate temperature might be due to the defects present in the as-deposited layers.

In general, the temperature dependent electrical resistivity of a semiconductor material can be ascribed by the equation (6):

$$\rho = \rho_0 \exp\left(\frac{E_a}{k_B T}\right) \tag{6}$$

where, ρ_0 is the pre-exponential factor, k_B is the Boltzmann constant (8.6173×10^{-5} eV K^{-1}) and E_a is the thermal activation energy at corresponding temperature T.

Figure 9 shows the plots of $\ln(\rho)$ versus $10^3/T$ of $SnS_{1-x}Se_x$ films, which were fitted linearly to evaluate the activation energy of the films from the slope of the plot ($E_a = 1000 \times \text{slope} \times k_B$). The evaluated E_a values are

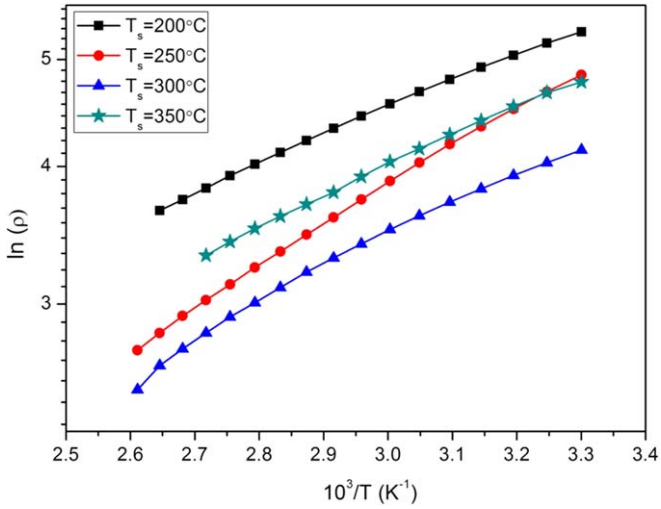

Figure 9. ln (ρ) versus 1/T plot for $SnS_{1-x}Se_x$ films deposited at different T_s.

Table 2. Electrical properties of $SnS_{1-x}Se_x$ films.

T_s (°C)	ρ (Ω-cm)	E_a (eV)
200	244.6	0.22
250	90.6	0.27
300	65.2	0.20
350	130.1	0.22

listed in table 2. The fall in E_a values indicates the reduced concentration of defect levels in the films caused by increase in substrate temperature.

3.5. Photosensitivity

The photoconductivity measurements were performed for $SnS_{1-x}Se_x$ films grown at $T_s = 300$ °C, since the films exhibited better optical and electrical properties than the other films. The photosensitivity (S) of $SnS_{1-x}Se_x$ layers can be calculated using the following relation (7), where σ_{light} is the photoconductivity and σ_{dark} is the dark conductivity of the layers [30].

$$S = \frac{\sigma_{light} - \sigma_{dark}}{\sigma_{dark}} \quad (7)$$

The variation in photosensitivity of $SnS_{1-x}Se_x$ films as a function of incident light intensity (L, mW/cm^2) is shown in figure 10. The photosensitivity was increased with increase of light intensity due to the increase in photo generated electron – hole pairs in the layers and thus the photoconductivity [31]. Moreover, the plot shows that photosensitivity (S) is linearly dependent on light intensity (L) by following power law with intensity, $S \propto L^{\gamma}$, where the parameter γ value indicates the nature of recombination (mono ($\gamma = 1$) or bimolecular ($\gamma = 0.5$) recombination) [32]. In the present case, γ is ~0.5 confirms the bimolecular recombination mechanism in the films. These results indicate that $SnS_{1-x}Se_x$ films are good photo-responsive and potential for solar cell applications.

4. Conclusions

$SnS_{1-x}Se_x$ thin films were deposited on glass substrates by thermal co-evaporation technique at different substrate temperatures (200 °C–350 °C). From the structural studies, the crystallinity of $SnS_{1-x}Se_x$ layers was improved with increase of substrate temperature. The optical measurements revealed that the band gap energy of the films varied between 1.59 eV and 1.46 eV with increase of substrate temperature from 200 °C to 350 °C. The Urbach energy of the layers was also decreased with increase of T_s and a minimum value of 178 meV was obtained at $T_s = 300$ °C, indicating low density of localized states in the band gap region. A slight increase of refractive index with a decrease of extinction coefficient was observed as the substrate temperature increased.

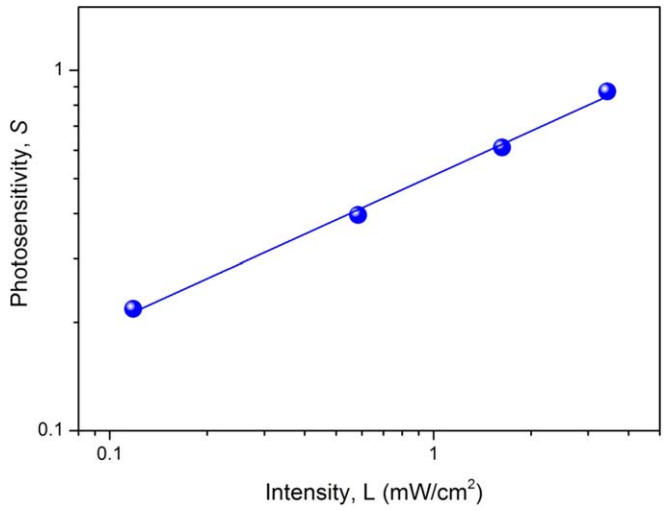

Figure 10. Variation of photosensitivity of $SnS_{1-x}Se_x$ films grown at $T_s = 300$ °C with light intensity.

From electrical measurements, it was inferred that the films deposited at $T_s = 300$ °C had lower resistivity and activation energy compared to other layers. Moreover, the photoconductivity measurements revealed that the films are sensitive to incident light and showed increased photosensitivity with light intensity. Further, the recombination in the films is observed to be bimolecular type. It is concluded from the above analysis that the films deposited at $T_s = 300$ °C with good optical and electrical properties can be used as an absorber layer in thin film solar cell applications.

Acknowledgments

The authors, Prof K T Ramakrishna Reddy and Prof M S Tivanov wish to acknowledge the Dept. of Science and Technology, Govt. of India (Grant no: DST/INT/BLR/P-30/2019) and State Committee on Science and Technology of the Republic of Belarus.

ORCID iDs

K Saritha https://orcid.org/0000-0003-4345-4937
S Rasool https://orcid.org/0000-0002-0807-9951

References

[1] Green M A, Emery K, Hishikawa Y, Warta W, Dunlop E D, Levi D H and Ho-Baillie A W Y 2016 Solar cell efficiency tables (Version 49) *Prog. Photovolt. Res. Appl.* **25** 3
[2] Jackson P, Wuerz R, Hariskos D, Lotter E, Witte W and Powalla M 2016 Effects of heavy alkali elements in Cu(In, Ga)Se_2 solar cells with efficiencies up to 22.6% *Phys. Status Solidi RRL* **10** 583
[3] Ravindran M and Praveenkumar C 2018 Status review and the future prospects of CZTS based solar cell – A novel approach on the device structure and material modelling for CZTS based photovoltaic device *Renew. Sustain. Energy Rev.* **94** 317
[4] Shin D, Saparov B and Mitzi D B 2017 Defect engineering in multinary earth-abundant chalcogenide photovoltaic materials *Adv. Energy Mater.* **7** 1602366
[5] Li J, Zhang Y, Zhao W, Nam D, Cheong H, Wu L, Zhou Z and Sun Y 2015 A temporary barrier effect of the alloy layer during selenization: tailoring the thickness of $MoSe_2$ for efficient $Cu_2ZnSnSe_4$ solar cells *Adv. Energy Mater.* **5** 1402178
[6] Li J, Wang D, Li X, Zeng Y and Zhang Y 2018 Cation substitution in earth-abundant kesterite photovoltaic materials *Adv. Sci.* **5** 1700744
[7] Sun K, Yan C, Liu F, Huang J, Zhou F, Stride J A, Green M and Hao X 2016 Over 9% efficient kesterite Cu_2ZnSnS_4 solar cell fabricated by using $Zn_{1-x}Cd_xS$ buffer layer *Adv. Energy Mater.* **6** 1600046
[8] Lee Y S, Gershon T, Gunawan O, Todorov T K, Gokmen T, Virgus Y and Guba S 2015 $Cu_2ZnSnSe_4$ thin film solar cells by thermal co-evaporation with 11.6% efficiency and improved minority carrier diffusion length *Adv. Energy Mater.* **5** 1401372
[9] Wang W, Winkler M T, Gunawan O, Gokmen T, Todorov T K, Zhu Y and Mitzi D B 2014 Device characteristics of CZTSSe thin film solar cells with 12.6% efficiency *Adv. Energy Mater.* **4** 1301465
[10] Albers W, Haas C, Ober H, Schodder G R and Wasscher J D 1962 Preparation and properties of mixed crystals $SnS_{(1-x)}Se_x$ *J. Phys. Chem. Solids* **23** 215
[11] Wei H, Su Y, Chen S, Lin Y, Yang Z, Chen X and Zhang Y 2011 Novel SnS_xSe_{1-x} nanocrystals with tunable band gap: experimental and first principles calculations *J. Mater. Chem.* **21** 12605
[12] Patel T H, Vaidya R and Patel S G 2003 Anisotropic behaviour of semiconducting tin monosulphoselenide single crystals *Bull. Mater. Sci.* **26** 569

[13] Im H S *et al* 2013 Facile phase and composition tuned synthesis of tin chalcogenide nanocrystals *RSC Adv.* **3** 10349
[14] Gao W, Li Y, Guo J, Ni M, Liao M, Mo H and Li J 2018 Narrow-gap physical vapour deposition synthesis of ultrathin $SnS_{1-x}Se_x$ ($0 \leqslant x \leqslant 1$) two-dimensional alloys with unique polarized Raman spectra and high (opto)electronic properties *Nanoscale* **10** 8787
[15] Dhanasekaran V, Sundaram K, Jung J and Mahalingam T 2015 Microstructural properties evaluation of SnSSe alloy films *J. Mater. Sci.: Mater. Elec.* **26** 1641
[16] Subramanian B, Sanjeeviraja C and Jayachandran M 2003 Materials properties of electrodeposited $SnS_{0.5}Se_{0.5}$ films and characterization of photoelectrochemical solar cells *Mater. Res. Bull.* **38** 899
[17] Kumar V, Sharma D K, Sharma K, Singh P and Dwivedi D K 2018 Preparation and characterization of screen printed $SnS_{0.5}Se_{0.5}$ alloy films *J. Mater. Sci., Mater. Electron.* **29** 846
[18] Banotra A and Padha N 2018 Development of $SnS_{0.4}Se_{0.6}$ ternary alloy on annealing of thermally deposited films *J. Electron. Mater.* **47** 1
[19] Barrios-Salgado E, Rodriguez-Guadarrama L A, Garcia-Angelmo A R, Alvarez J C, Nair M T S and Nair P K 2016 Large cubic tin sulphide-tin selenide thin film stacks for energy conversion *Thin Solid Films* **615** 415
[20] Barrios-Salgado E, Rodriguez-Guadarrama L A, Garcia M L R, Martinez L G, Nair M T S and Nair P K 2017 Thin film solar cells of cubic structured SnS-SnSe *Phys. Status Solidi a* **1700036** 1
[21] Shoroder D K 1990 *Semiconductor Materials and Device Characterization* (New York: Wiley) ISBN:978-0-471-74908-0
[22] Chalapathi U, Uthanna S and Sundara Raja V 2017 Structural, microstructural and optical properties of Cu_2ZnSnS_4 thin films prepared by thermal evaporation: effect of substrate temperature and annealing *Bull. Mater. Sci.* **40** 887
[23] Ahn S, Jung S, Gwak J, Cho A, Shin K, Yoon K, Park D, Cheong H and Yun J H 2010 Determination of band gap energy (E_g) of $Cu_2ZnSnSe_4$ thin films: on the discrepancies of reported band gap values *Appl. Phys. Lett.* **97** 021905
[24] Basak A, Mondal A and Singh U P 2016 Impact of substrate temperature on the structural, optical and electrical properties of thermally evaporated SnS thin films *Mater. Sci. Semicond. Proc.* **56** 381
[25] Indirajith R, Srinivasan T P, Ramamurthi K and Gopalakrishnan R 2010 Synthesis, deposition and characterization of tin selenide thin films by thermal evaporation technique *Curr. Appl Phys.* **10** 1402
[26] Tauc J 1970 *Optical Properties of Solids* (Amsterdam: North-Holland) 903
[27] Zhao L, Di Y, Yan C, Liu F, Cheng Z, Jiang L, Hao X, Lai Y and Li J 2016 *In situ* growth of SnS absorbing layer by reactive sputtering for thin film solar cells *RSC Adv.* **6** 4108
[28] Hassanien A S and Akl A A 2016 Effect of Se addition on optical and electrical properties of chalcogenide CdSSe thin films *Superlattices Microstruct.* **89** 153
[29] Nehra S P, Chander S, Sharma A and Dhaka M S 2015 Effect of thermal annealing on physical properties of vacuum evaporated In_2S_3 buffer layer for eco-friendly photovoltaic applications *Mater. Sci. Semicond. Process.* **40** 26
[30] Mahato S and Kar A K 2017 The effect of annealing on structural, optical and photosensitive properties of electrodeposited cadmium selenide thin films *J. Science: Adv. Mater. Devices* **2** 165
[31] Henry J, Mohanraj K and Sivakumar G 2017 Effect of pH-induced on the photosensitivity of non-toxic Cu_2ZnSnS_4 thin film by chemical bath deposition *Optik* **141** 139
[32] Neetu and Zulfequar M 2014 Photoconductivity of $Se_{90-x}Te_{10}Zn_x$ thin films *Indian J. Pure & Apmpl. Phys.* **52** 53 http://nopr.niscair.res.in/handle/123456789/25143